Journal of Energy Chemistry 37 (2019) 117–125

Contents lists available at ScienceDirect

Journal of Energy Chemistry

journal homepage: www.elsevier.com/locate/jechem

http://www.journals.elsevier.com/journal-of-energy-chemistry/

Enhanced coking resistance of a Ni cermet anode by a chromates protective layer☆

Hong Chang[a], Huili Chen[a,*], Guangming Yang[b], Wei Zhou[b], Jianping Bai[d], Sidian Li[a], Zongping Shao[b,c]

[a] Institute of Molecular Science, Key Laboratory Material Energy Conversion & Storage Shanxi Province, Shanxi University, Taiyuan 030006, Shanxi, China
[b] State Key Laboratory of Materials-Oriented Chemical Engineering, College of Chemistry & Chemical Engineering, Nanjing University of Technology, No. 5 Xin Mofan Road, Nanjing 210009, Jiangsu, China
[c] Department of Chemical Engineering, Curtin University, Perth, WA 6845, Australia
[d] State Key Laboratory of Coal and CBM Co-Ming, Shanxi Lanyan Coalbed Methane Group Co. Ltd, Jincheng 048204, Shanxi, China

ARTICLE INFO

Article history:
Received 27 September 2018
Revised 10 December 2018
Accepted 15 December 2018
Available online 18 December 2018

Keywords:
Solid oxide fuel cell (SOFC)
Ni cermet anode
Methane-based fuels
Chromates catalyst
Coking resistance

ABSTRACT

Ni-based anodes of SOFCs are susceptible to coking, which greatly limits practical application of direct methane-based fuels. An indirect internal reformer is an effective way to convert methane-based fuels into syngas before they reach anode. In this work, catalytic activity of a redox-stable perovskite $La_{0.7}Sr_{0.3}Cr_{0.8}Fe_{0.2}O_{3-\delta}$ (LSCrFO) for methane conversion was evaluated. The catalyst was fabricated as an anodic protective layer to improve coking resistance of a Ni cermet anode. Using wet CH_4 as a fuel, the LSCrFO-modified cell showed excellent power output and good coking resistance with peak power density of 1.59 W cm^{-2} at 800 °C. The cell demonstrated good durability lasting for at least 100 h. While the bare cell without the protective layer showed poor durability with the cell voltage fast dropped from 0.75 V to 0.4 V within 30 min. Under wet coal bed methane (CBM) operation, obvious performance degradation within 35 h (1.7 mV h^{-1}) was observed due to the influence of heavy carbon compounds in CBM. The pre- and post-mortem microstructures and carbon analysis of the anode surface and catalyst surface were further conducted.

1. Introduction

Solid oxide fuel cells (SOFCs) have attracted a lot of attention in recent years due to their minimal emission of pollutants and high conversion efficiency [1–3]. In addition, SOFC exhibits admirable fuel flexibility. It can work on any kind of fuel, including H_2, biofuels, hydrocarbons, diesel, natural gas, coal, etc. [4–7]. Up to now, 8% yttria-stabilized zirconia (YSZ) is the most extensively applied electrolyte material because of its proper oxygen ion conductivity, appropriate mechanical strength and decent chemical and thermal stability under SOFC operating conditions. The state-of-art SOFC anode material is Ni-YSZ cermet because of its good electro-catalytic activity for the H_2 oxidation and proper, high mixed electronic-ionic conductivity, etc. However, some drawbacks such as poor redox-stability [8], coking for hydrocarbon [7], and poisoning for sulfur-containing fuels [9], are observed. Coking occurs when hydrocarbon fuels are used, which blocks the Ni active sites present at the anode and decreases the catalytic activity of anode, more seriously, deteriorates the cell [10]. To address this problem, an effective method is to apply a catalytic layer on anode surface to mitigate carbon deposition and anode poisoning by undesired contaminants [11–14]. Recently much attention has been focused on applying mixed-valent and oxygen-deficient perovskites to catalyze hydrocarbon conversion [15–19]. In a typical cubic perovskite structure of ABO_3, large A ions in a 12-coordinated site, usually are lanthanide metals, alkaline earth metals, or rare earth metals. Whereas B ions in a 6-coordinated site, usually are the first-row transition metals, such as Cr, Fe, Mn, Co, or a mixture thereof. The catalytic ability usually relies on B site ions. However, A ions also affect the total catalytic ability of perovskite materials, principally by influencing the oxidation of B ions therefore changing the redox ability of perovskite materials [20]. In our

☆ This work was supported by the Coal Seam Gas Joint Foundation of Shanxi (2015012016); Shanxi Province Science Foundation (2016011025); Shanxi Scholarship Council of China (2016-010); Shanxi "1331 Project" Key Innovative Research Team ("1331KIRT") and the Open Funding from State Key Laboratory of Material-oriented Chemical Engineering (No. KL16-03). Thanks scientific instrument center of Shanxi University for the SEM test.

* Corresponding author.
E-mail address: huilichen@sxu.edu.cn (H. Chen).

https://doi.org/10.1016/j.jechem.2018.12.007

previous work [21,22], perovskites $La_{0.8}Sr_{0.2}Co_{0.4}Fe_{0.6}O_3$ (LSCF) and $Sr_2MoFeO_{6-\delta}$ (SMFO) were applied as an anodic protective layer. Although durability is greatly improved, some issues must be addressed further. For example, under SOFC conditions, LSCF is unstable and is reduced to (Sr,La)FeO_4 and CoFe alloy nanoparticles. SMFO is stable at low oxygen partial pressure, but it becomes unstable in air and decomposes into $SrMoO_4$ and $SrFeO_{3-\delta}$ when temperatures are above 400 °C [23], which influences the catalytic activity. Besides, it was reported that at low temperatures SMFO could react with water to form $Sr(OH)_2$, restricting its potential applications in fuel cells [24]. Recently, the doped lanthanum chromates, such as $La_xSr_{1-x}Cr_yM_{1-y}$ (M = Co,Fe,Mn), have been proved to be heterogeneous catalysts with good redox stability and catalytic activity, and have been used as electrodes for SOFC and SOEC [25,26]. These perovskites run well in reducing and oxidizing atmospheres and can be applied as anode and cathode materials [22,27]. For example, $(La_{1-x}Sr_x)$ $(Cr_yFe_{1-y})O_{3-\delta}$ was reported to have high catalytic activity for CH_4 reforming, electrical conductivity and desirable redox stability when Fe concentration was lower than 50% ($y \geq 0.5$) [26,27].

In this work, a pure redox-stable perovskite $La_{0.7}Sr_{0.3}Cr_{0.8}Fe_{0.2}O_{3-\delta}$ (LSCrFO) was prepared using a typical sol-gel method. Its catalytic activity for CH_4 partial oxidation, CO_2 and steam reforming was evaluated. A Ni–YSZ anode-supported cell with an independent LSCrFO catalyst layer was fabricated. Electrochemical performance and durability of the LSCrFO-modified cell were tested operating on wet methane and wet coal bed methane (CBM) fuels.

2. Experimental

2.1. Sample preparation

$La_{0.7}Sr_{0.3}Cr_{0.8}Fe_{0.2}O_{3-\delta}$ (LSCrFO), $Ba_{0.5}Sr_{0.5}Co_{0.8}Fe_{0.2}O_{3-\delta}$ (BSCF) and $La_{0.7}Sr_{0.3}MnO_{3-\delta}$ (LSM) were synthesized using a conventional sol-gel method. Herein, we take LSCrFO as an example. $La(NO_3)_3{\cdot}6H_2O$, $Sr(NO_3)_2$, $Fe(NO_3)_3{\cdot}9H_2O$ and $Cr(NO_3)_3{\cdot}9H_2O$ were used as starting materials and were dissolved in EDTA-$NH_3{\cdot}H_2O$ solution in required amounts according to stoichiometry. Under successive stirring and heating, citric acid (CA) was added with the total mole ratio of M^{n+}(total metal ions):EDTA:CA equal to 1:1:2. Subsequently, the pH value of the solution was adjusted to be about 7 by $NH_3{\cdot}H_2O$. The solution was churned and heated at 70 °C to evaporate the solvent slowly until the gel formed. The gel was treated at 250 °C for 8 h to remove the organic substance. Then the precursor powders were ground with a mortar and were calcined at 1100 °C for 2 h, thus the desired perovskite-type LSCrFO was obtained.

The catalyst/support dual-layered disc was prepared by a dry-pressing/co-sintering process. Al_2O_3 and PVB (at a weight ratio of 25:3) were ball-milled in alcohol for 1 h. After being dried, the resulting sample (0.25 g) was dry-pressed in a steel die (13 mm diameter) to form a support layer. Then 0.03 g of catalyst powder (70 wt% LSCrFO + 10 wt% graphite + 20 wt% PVB) was spread on the support layer and co-pressed, and subsequently calcined in air for 5 h at 900 °C.

A high temperature SOFC (HT-SOFC) with the structure of NiO–YSZ/YSZ/LSM–YSZ was fabricated, in which the bi-layered anode/electrolyte half cell was prepared by co-pressing method, denoted as CP (Ni–YSZ)∼LSM. Firstly 0.4 g of powders of YSZ, NiO and starch in a weight ratio of 6:4:1 were ball-milled in alcohol at 200 rpm for 1 h. After being dried, the resulting powders were dry-pressed in a steel die (15 mm diameter) at 68 MPa for 30 s to form an anode layer. Whereafter, 0.025 g of YSZ powder was co-pressed with the anode layer at 200 MPa for 1 min to form the bi-layered anode/electrolyte slice followed by annealing in air at 1400 °C for 5 h. The cathode slurry with the cathode powders (70 wt% LSM + 30 wt% YSZ) and a mixed solution of glycerol, ethylene glycol and isopropyl alcohol was ball-milled at 350 rpm h^{-1} speed. Then the slurry was sprayed on the surface of the dense YSZ electrolyte using an air gun with a circular area of 0.478 cm^2 and subsequently was sintered at 1100 °C for 2 h. Silver slurry as current collector was painted on the surface of the cathode layer. Silver wires were stuck to the anode surface and the cathode surface to conduct current. Thus a membrane-electrode-assembly (MEA) was completed. Fabrication process of a catalyst-modified cell was as followings: firstly, a catalyst/support dual-layered disc was fixed on a quartz tube by some silver paste, in which the catalyst was towards the inner of tube. Then a MEA was placed over the catalyst/support disc with the anode side towards the support layer and subsequently was sealed by the sealant. The fuel cell test setup is referenced to our recent paper [20,21].

Cells with and without LSCrFO were designated "LSCrFO//NiO–YSZ" and "NiO–YSZ", respectively. In this paper, a medium temperature SOFC (MT-SOFC) with the structure of NiO–YSZ/YSZ/SDC/BSCF–SDC was also fabricated, in which the anode layer was prepared via tape-casting, denoted as TP (Ni–YSZ)∼BSCF. Detailed fabrication process was given elsewhere [11].

2.2. Characterizations

Phase structures of the as sintered and reduced LSCrFO powders were characterized by XRD (X-ray powder diffraction, an Ultima (Rigaku D/Max-RB, Japan) apparatus worked at 35 mA and 40 kV using Cu $K\alpha$ radiation). The diffraction spectra were recorded in the 2θ range of 10°–80° with a rate of 5° min^{-1} per step and the corresponding data were analyzed by the JADE 6.0 software. Microstructures and morphologies of the electrodes and the catalysts were acquired using a scanning electron microscope (SEM, JEOL, JSM-7001F, Japan) with a Bruker (Germany) energy dispersive X-ray spectroscopy (EDX) detector.

Electrochemical performances of the cell were tested via an Iviumstat electrochemical workstation using a four-probe method. Prior to the test, H_2 was fed into the cell to in situ reduce the catalyst and the Ni cermet anode. During the measurement, H_2 or wet CH_4 or wet CBM was continuously fed into the anode compartment with an 80 mL min^{-1} flow rate (STP). The cathode was exposed to air directly. The electrochemical impedance spectra (EIS) were measured under a dc potential with an amplitude of 10 mV and a frequency range of 10^5–0.1 Hz at open circuit voltage (OCV).

2.3. Catalytic activity

The catalytic activity of the reduced LSCrFO for methane conversion was measured with a fixed-bed reactor at different temperatures. The catalyst (200 mg) supported by some silica wool was loaded into the constant temperature zone of the tube equipped with a thermocouple near the catalyst. A gas mixture (V_{CH4}:V_{O2} = 1:1, V_{CH4}:V_{H2O} = 1:2, V_{CH4}:V_{CO2} = 1:2) with a pressure of 6 MPa was used for methane partial oxidation (MPO), methane steam reforming (MSR) and methane dry reforming (MDR) with a CH_4 10 mL min^{-1} flow rate. For MSR, steam was fed into the reactor by a microsyringe pump. After the temperature was stable for 0.5 h, the composition of the outlet gas was analyzed by a gas chromatograph (Agilent 7820), which was equipped with a Poraplot Q, a Hayesep Q, a 5 A molecular sieve column and a thermal conductivity detector for the separation and detection of CO, CO_2, H_2, O_2 and CH_4. The CH_4 conversion and CO selectivity were calculated using the relevant method [28].

3. Results and discussion

3.1. Characterization of catalyst

Fig. 1(a) shows the XRD patterns of as sintered LSCrFO (LSCrFO-ox) and reduced LSCrFO (LSCrFO-re) which was treated under a hydrogen atmosphere at 850 °C for 2 h. After calcination in air at 1100 °C for 2 h, LSCrFO-ox powder presented a well-developed crystalline. All peaks can be well indexed as a single phase perovskite [29] and matched well with the standard PDF card of perovskite-type $LaFeO_3$ (PDF # 37-149,311). 80 mol% of Cr cations doping on B-site of $LaFeO_3$ had no significant influence on the main peaks of the perovskite oxide. Besides, it is well known that the anodic catalytic material should have good phase structure stability in a reducing atmosphere at high temperature. After reducing at 850 °C for 2 h, no any impurity phase was detected while LSCrFO-re maintained a perovskite-type structure, indicating LSCrFO material had good redox stability at such a high temperature. Compared with $LaFeO_3$ (PDF # 37-149,311), the peak at $2\theta = 32.19°$ was slightly moved to a higher angle at 32.34° and 32.40° for LSCrFO-re and LSCrFO-ox, respectively (Fig. 1(b)), which is indicative of lattice distortion and decrease of the cell parameters [30–32]. Average particle sizes of ca. 23.2 nm and 33.4 nm were observed for LSCrFO-ox and LSCrFO-re, respectively. XRD results demonstrate the feasibility of LSCrFO being applied as a stable catalyst material under SOFC condition.

3.2. Characteristic of the LSCrFO-modified cell

Fig. 2 shows an illustration of the LSCrFO-modified cell test setup. The catalyst layer was adjacent but separated from the anode of the cell. Current was conducted by the Ag wire from the anode and cathode. In this case, the conductivity of the Ni-based anode was not influenced by the non-conductive catalyst. Thus, this dual layer would not affect the cell resistance.

In this SOFC assembly, it is believed that wet methane-based fuels would be partially reformed to CO and H_2 by the catalyst layer before they reach the Ni-based anode. Simultaneously, vapor which is required in the reforming reaction is provided by the product from the electrochemical oxidation of H_2 and the bubbling water. What's more, the catalyst layer would function as a diffusion barrier layer. As a result, some unreformed fuels would be flown out along with the off gas. Therefore, coking on the Ni-based anode can be reduced because methane concentration near anode surface would greatly decrease. It is also clear that the products H_2 and CO can diffuse more easily than CH_4 molecule. As mentioned above, the LSCrFO-modified cell could improve the performance compared with the bare cell when fueled with methane-based gas.

The catalyst layer was composed of 60 μm catalyst and 1.3 mm support. The pore parameters and specific surface area of the catalyst layer were characterized using nitrogen adsorption/desorption. Fig. 3 shows the nitrogen adsorption/desorption isotherms and the BJH pore size distribution pattern of the dual-layered catalyst/support disc. The specific surface area and the pore volume were 51.1 $m^2\ g^{-1}$ and 0.16 $cm^3\ g^{-1}$, respectively. The dual-layered catalyst disc exhibited a mesoporous structure with a typical type-H3 hysteresis loop. The average pore size was about 8.9 nm (inset).

3.3. Catalytic performance

As an ideal catalyst for SOFC operating on methane-based fuels, the material should have high catalytic activity for methane conversion. Under SOFC condition, probably MPO, MSR and MDR co-exist. Therefore, the catalytic activities of LSCrFO-re towards MPO, MSR and MDR were measured in the temperature range of

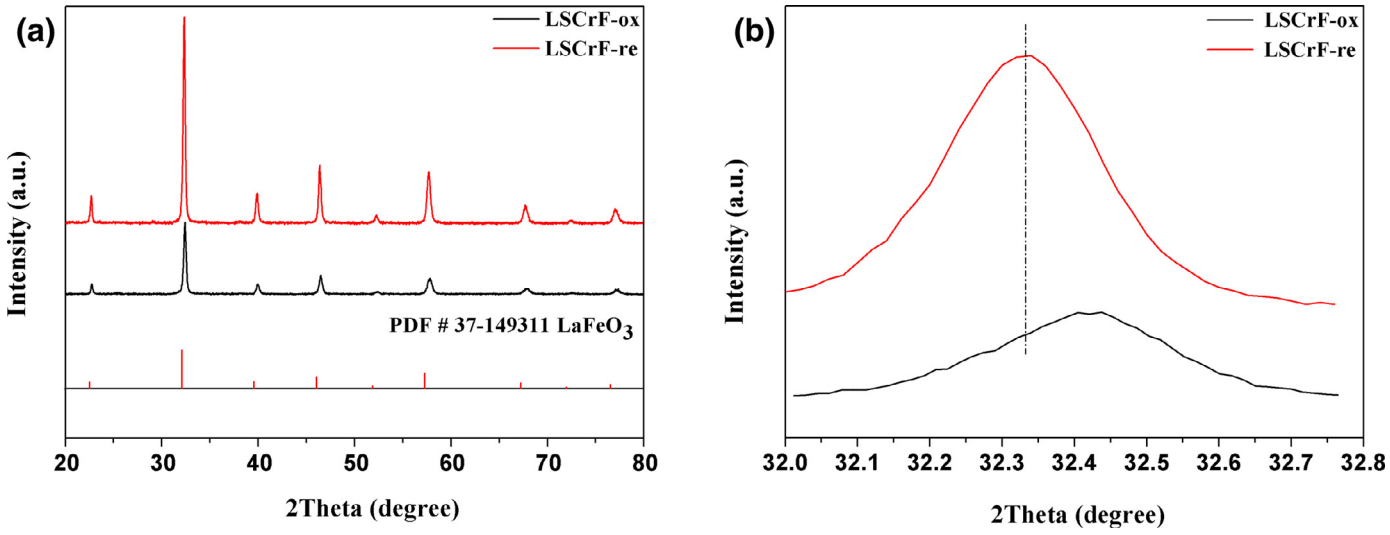

Fig. 1. The whole (a) and expanded (b) XRD patterns of LSCrFO-ox, LSCrFO-re and $LaFeO_3$.

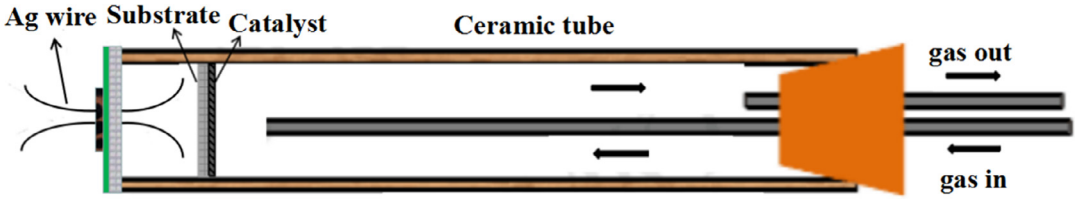

Fig. 2. Illustration of the catalyst-modified cell test setup.

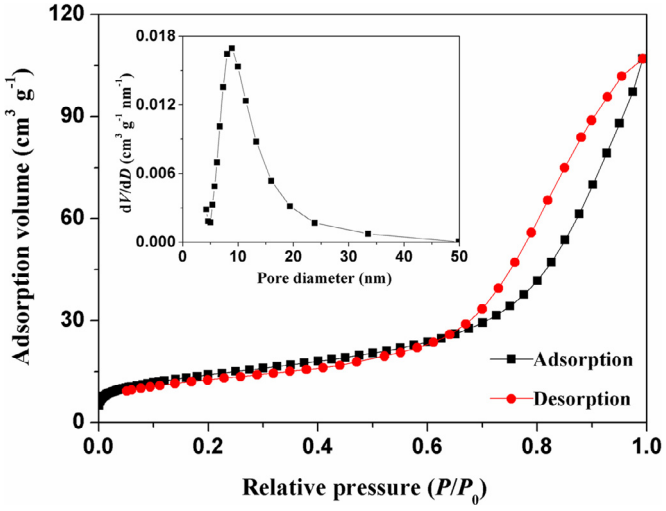

Fig. 3. The nitrogen adsorption/desorption isotherms curves and the BJH pore size distribution pattern of LSCrFO-ox-Al_2O_3 double-layered disc.

700–900 °C, as shown in Fig. 4. As the temperatures rose, CH_4 conversion and CO selectivity increased greatly. At 900 °C, CH_4 conversion reached about 65.7%, 43.2% and 54.6% with CO selectivity of 78.5%, 95.7%, and 74.5% for MPO, MSR and MDR, respectively. LSCrFO-re exhibited moderate catalytic properties toward methane conversion.

3.4. Cell performance

An anode-supported cell with high stability (NiO–YSZ/YSZ/LSM–YSZ) is used to achieve good re-productivity. In order to assess coking resistance of the LSCrFO-modified cell (LSCrFO//NiO–YSZ), wet CH_4 and wet CBM (composition: CH_4, 82.9975%; C_2–C_8, 3.4731%; N_2, 10.1839%; CO_2, 1.1602%; O_2, 2.1853%) were used as the fuels. A bare cell without the catalyst layer (NiO–YSZ) was used for comparison purpose. The I-V(P) curves of cells when operating on wet CH_4 and wet CBM are shown in Fig. 5. With the increment of temperatures, peak power densities (PPD) of all cells increased monotonously, which was attributed to an increment of the O^{2-} conductivity of YSZ and the catalytic activity of the electrodes at higher temperatures. For example, with temperature elevated up from 750 to 850 °C, PPDs of [(NiO–YSZ)-CH_4] increased dramatically from 0.20 to 0.55 W cm^{-2} (Fig. 5(a)). While PPDs of [(LSCrFO//Ni–YSZ)–CH_4] increased dramatically from 0.27 to 0.66 W cm^{-2} accompanied by an increment of current densities from 1.35 to 2.7 A at the corresponding temperatures (Fig. 5(b)). PPDs showed increment of 35%, 5.9% and 20% at 750 °C, 800 °C and 850 °C. The wave-shape increment of PPDs from 750 °C to 850 °C maybe was explained as followings. Under the actual SOFC working conditions, in addition to the reactions of methane reforming, methane cracking also occurred meanwhile. Cell performance was a balance of methane reforming and methane cracking. Thermodynamically, methane decomposed into carbon and hydrogen at temperatures above 547 °C. Moreover, carbon deposits increased with elevating temperatures [33]. Thus, carbon deposition was more severe at 800 °C than that at 750 °C. In this work, for [(LSCrFO//Ni–YSZ)–CH_4], methane cracking dominated at temperatures below 800 °C because LSCrFO had low catalytic activity with CH_4 conversion of 7.66 % at 800 °C for MSR, which was proved by the above catalytic test. With temperatures increasing to 850 °C, CH_4 conversion due to MSR reached 37%, which partially reduced the effect of carbon deposits produced by methane cracking. Therefore, the amount of increase in PPD enhanced at 850 °C.

Fig. 6 provides the comparison of I-V(P) curves for the cells with and without the LSCrFO catalyst layer operating on wet CH_4 and wet CBM at 850 °C, respectively. Application of the LSCrFO catalyst layer improved the cell performance. For CH_4 fuel, PPDs for [(LSCrFO//Ni–YSZ)–CH_4] and [(Ni–YSZ)–CH_4] were 0.66 and 0.55 W cm^{-2}, respectively. For CBM fuel, PPDs for [(LSCrFO//Ni–YSZ)–CBM] and [(Ni–YSZ)–CBM] were 0.59 and 0.55 W cm^{-2}, respectively. Probably the increased PPDs came from the H_2 electrochemical oxidation, which was ascribed to a fuel pre-forming process from methane to CO and H_2 by the LSCrFO catalyst layer. In addition, at low current density, there was a lower voltage loss for the catalyst-modified cells, which indicates a smaller electrode resistance [21]. Except the catalyst layer, these cells have the same cell configuration, cell materials and cathode atmosphere. Therefore the difference on the electrode resistance should come from the anode atmosphere. The results further reveal that the CH_4-based fuels have been partially confirmed to CO and H_2 by the catalyst layer, which have a lower electrode polarization [21].

Electrochemical impedance spectra (EIS) were also recorded at different temperatures. Usually, the intercepts at the high frequency and low frequency with the real axis, approximately equal

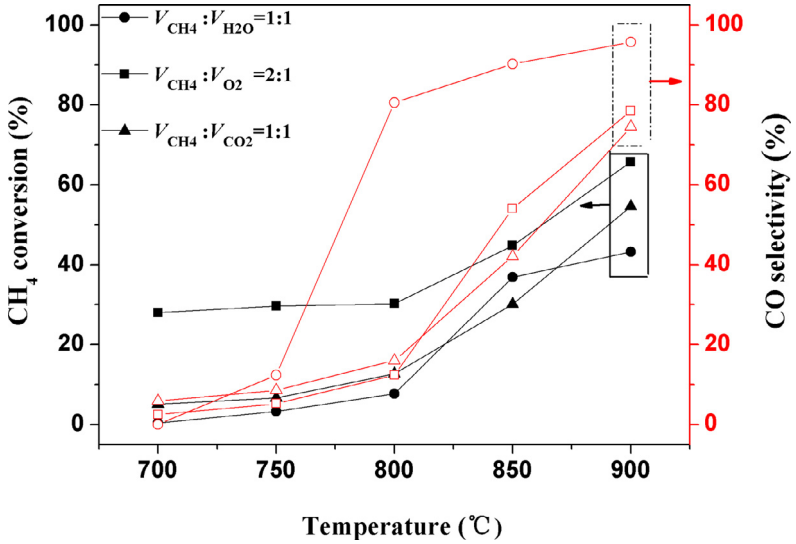

Fig. 4. Catalytic activity of LSCrFO-re for MPO ($V_{CH4}:V_{O2}=2:1$), MSR ($V_{CH4}:V_{H2O}=1:1$) and MDR ($V_{CH4}:V_{CO2}=1:1$).

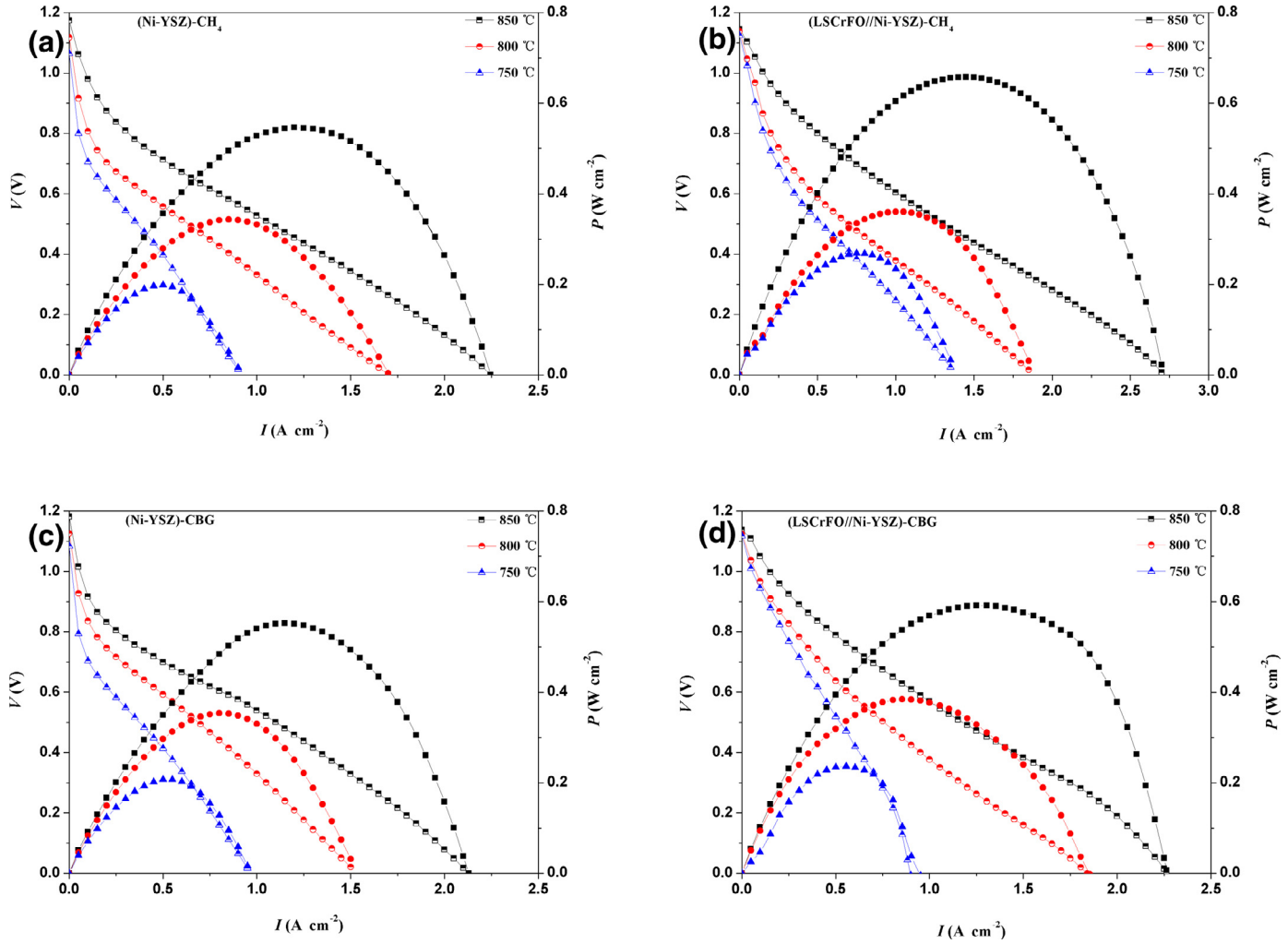

Fig. 5. The I-V(P) curves of the cells without (a & c) and with (b & d) the LSCrFO catalyst layer when operating on wet CH_4 and wet CBM fuel at different temperatures.

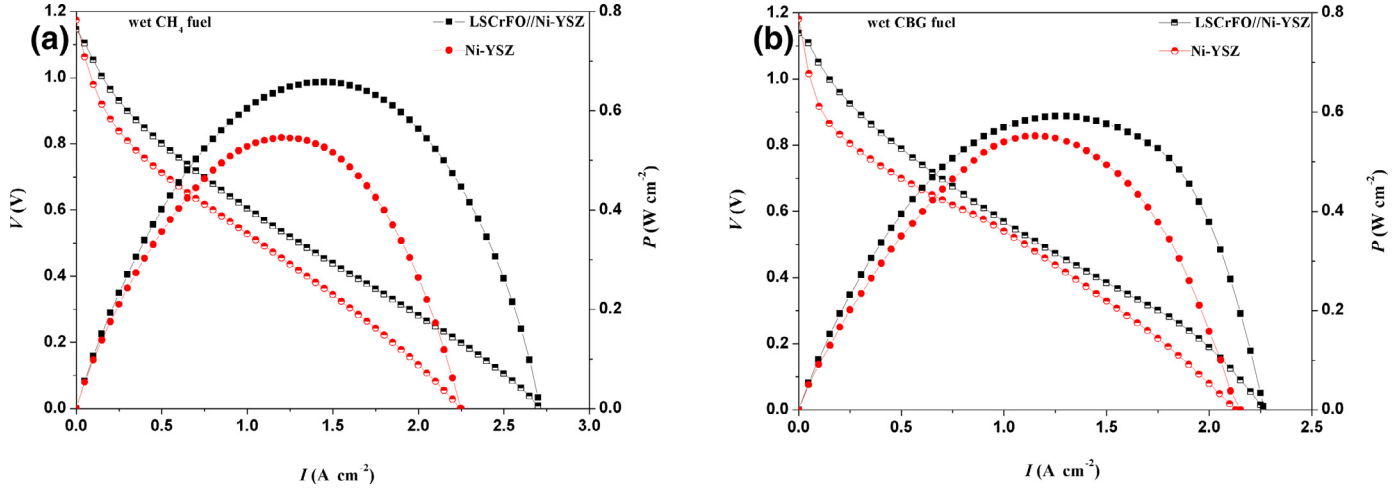

Fig. 6. The comparison of I-V(P) curves for the cells with and without the LSCrFO catalyst layers operating on wet CH_4 (a) and wet CBM (b) at 850 °C.

to ohmic (R_Ω) and total (R_T) resistances, respectively. R_Ω is mainly ascribed to the experimental setup and the ion resistance from electrolyte, which is thought to have identical values in this work due to the same cell structure and cell materials, which is also proved by experiments (Fig. 7(a)). While the polarization resistance (R_P), corresponding to the difference between R_Ω and R_T, consists of two processes, located at low frequencies (LF) and high frequencies (HF). The high-frequency resistance (R_{HF}) is usually ascribed to an electrochemical process at the electrolyte/electrode interface, while the low-frequency resistance (R_{LF}) is often associated with a mass transport process [29,34,35]. Fig. 7(a) illustrates the representative open-circuit impedance spectra for [(LSCrFO//Ni–YSZ)–CH_4] and [(Ni–YSZ)–CH_4] at 850 °C. Compared with [(Ni–YSZ)–CH_4], the polarization resistance (R_P) of [(LSCrFO//Ni–YSZ)–CH_4] signifi-

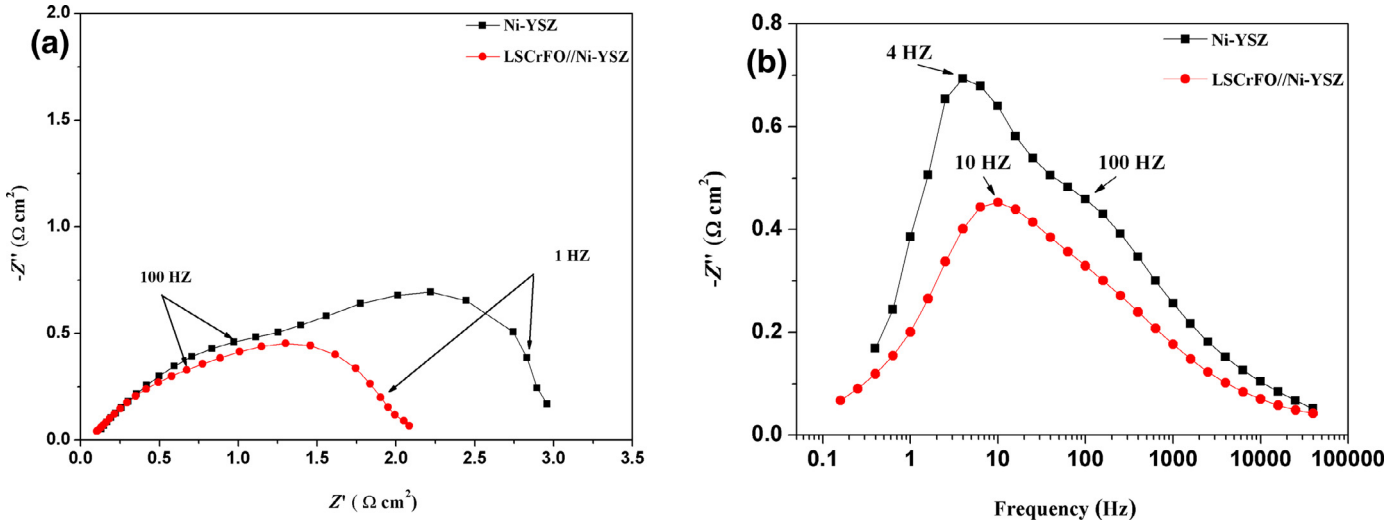

Fig. 7. Comparison of the Nyquist plot (a), and bode plot (b), of EIS for the cells with and without the LSCrFO catalyst layer at 850 °C under wet CH_4 operation, respectively.

cantly decreased. For example, the R_P values were about 1.98 and 2.82 Ω cm^2 for [(LSCrFO//Ni–YSZ)–CH_4] and [(Ni–YSZ)–CH_4] at 850 °C, respectively. The reduced R_P accounted for the high performance of the catalyst-modified cell. In the Bode plot of Fig. 7(b), [(LSCrFO//Ni–YSZ)–CH_4] showed a lower impedance in the whole frequency domain than [(Ni–YSZ)–CH_4], especially in the LF range. [(Ni–YSZ)–CH_4] showed two summits at about 4 Hz and at 100 Hz in the whole frequency. While [(LSCrFO//Ni–YSZ)–CH_4] showed only one summit at 10 Hz. Simultaneously, the Bode plots of EIS for [(LSCrFO//Ni–YSZ)–CH_4] showed summits at 16 Hz and 10 Hz at 750 and 800 °C, respectively (Fig. S1). Above results indicate a diffusion-controlled process because it is weakly affected by the temperature. Impedance analysis indicates that the catalyst layer not only speeds up the electrochemical progress, but also promotes the gas diffusion because H_2 has a lower electrode polarization and a smaller size than CH_4.

A MT-SOFC with the structure of LSCrFO//TP (Ni–YSZ)∼BSCF was also fabricated. Operating on wet CH_4, the cell demonstrated promising performance, generating PPD of 1.59 W cm^{-2} at 800 °C (Fig. 8), which was a remarkable improvement comparing with the HT-SOFC with the configuration of LSCrFO//CP (Ni–YSZ)∼LSM, about 0.36 W cm^{-2}.

3.5. The durability tests in galvano-static mode under wet CH_4 and wet CBM

In addition to high electrochemical performance, durability is another essential requirement for direct methane-fuelled SOFCs. To assess the durability of the catalyst-modified cells, they were subjected to methane-based fuels in galvano-static mode at 333 mA cm^{-2} and 850 °C as shown in Fig. 9. A bare cell was used for a comparison. Without protection of the catalyst layer, the bare cell showed poor durability. The voltage in wet CH_4 and wet CBM fuels rapidly decreased within 30 min. In contrast the LSCrFO-modified cell exhibited excellent stability within 100 h under wet CH_4 operation. Clearly, the voltage decreased in the initial 8 h and then increased and stabilized at about 0.71 V in the coming period. While for wet CBM, a voltage drop (1.7 mV h^{-1}) was observed for the LSCrFO-modified cell within 35 h. Because there was 3.4731% C_2–C_8 in CBM, carbon deposits came from CH_4 and heavy hydrocarbon complexes. The instability of the voltage on CBM indicates that LSCrFO has low catalytic activity for oxidation of heavy hydrocarbon compounds, which is in line with that LSCF [21]. More carbon deposits were produced in a short time. The results reveal that application of the LSCrFO catalyst layer improves durability of SOFC with Ni cermet anode under a direct methane feeding mode.

3.6. Post-mortem microstructural analyses of cells

Fig. 10 displays the surface morphologies of the anode and catalyst layer before and after the durability tests in wet CH_4 and in wet CBM. It is obvious that the anode surface of the bare cell was porous before test (Fig. 10(a)), while after exposure to wet CH_4 for about 30 min, a close-grained morphology was observed (Fig. 10(b)). For the LSCrFO-modified cells, the surfaces of the anode and catalyst of the LSCrFO-modified cells maintained the porous structure after the durability test although sintering to some extent occurred (Fig. 10(c)–(f)). Simultaneously, porous anode and cathode layers maintained, and kept in compact touching with the densified electrolyte layer for the LSCrFO-modified cell after the durability test (Fig. S2). Above results indicate that the application of an independent LSCrFO catalyst layer improves coking resistance of the Ni cermet anode.

Further, from the EDX analysis (Table 1), after operation on wet CH_4 over 100 h, the related mean-carbon-contents (MCC) of the anode surface and the catalyst surface of the LSCrFO-modified cell were about 18.61 at% and 7.34 at%, respectively. While MCCs on the fresh anode surface and catalyst surface were 22.4 at% and 6.38 at%, respectively. After operation on wet CBM for 35 h, MCC on the anode surface was 42.34 at% which was higher than that on wet CH_4 under the same condition. This was attributed to the influence of the heavy carbon compounds in CBM. All of the above-mentioned results provide evidence that the application of the LSCrFO catalyst layer could improve coking resistance of a Ni–YSZ anode. Indeed, the independent catalyst layer could perform not only as a catalyst for fuel pre-reforming, but also as a protection layer to avoid direct contact between methane and the Ni-based anode. Therefore the probability of CH_4 cracking on Ni particles greatly decreased.

It is clear that under wet CH_4 condition, the LSCrFO-modifed cells showed high durability, although LSCrFO exhibits medium catalytic performance for MPO, MSR and MDR. Usually, a fixed-bed reactor could not really reflect the actual reaction of the fuel cell. In our recent paper [36], Ni/BaO/CeO_2 (NBC) showed high catalytic activity in a fixed-bed reactor with 75% CH_4 conversion efficiency at 800 °C for MSR. While gaschromatography (GC) analysis of tail gases from the operating NBC-modified cell showed that CH_4 conversion was only 21.7% at 0.16 A current load under wet CH_4 at

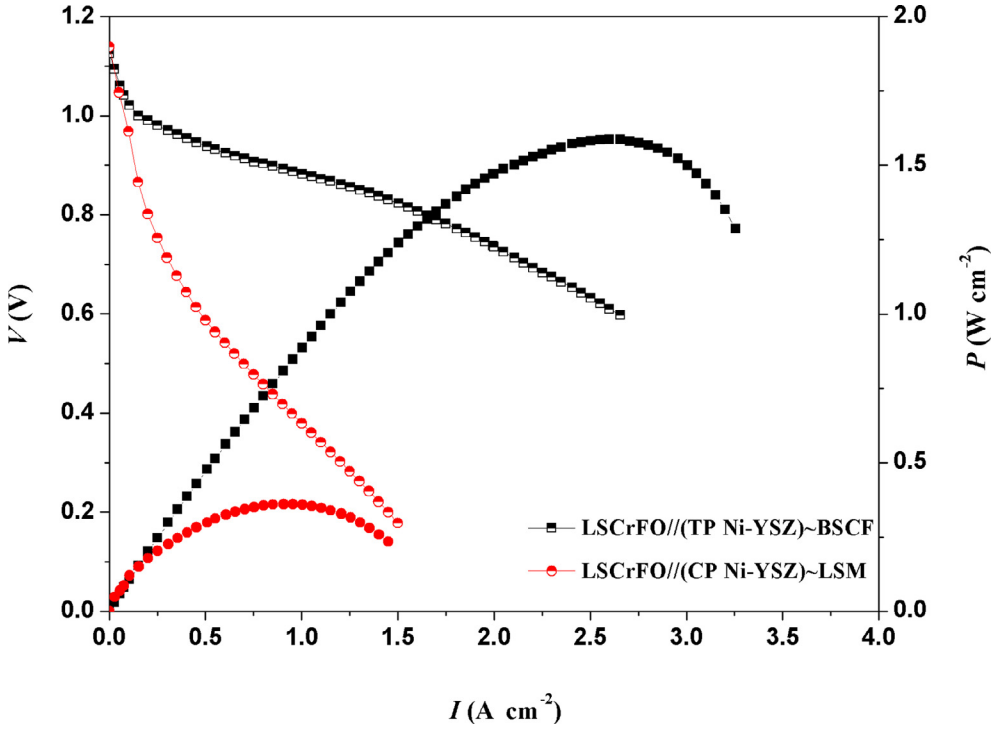

Fig. 8. Comparison of the electrochemical performance of LSCrFO//CP (Ni–YSZ)~LSM and LSCrFO//TP (Ni–YSZ)~BSCF when operating on wet CH_4 at 800 °C.

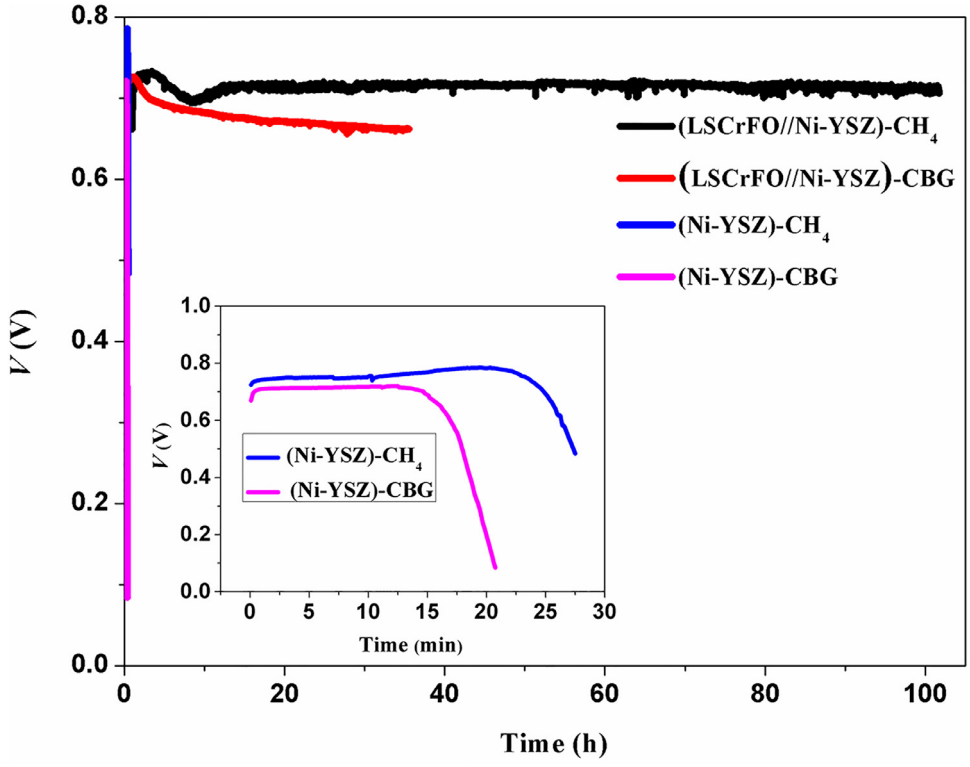

Fig. 9. The variation of voltages with time for the cells with and without the LSCrFO catalyst layer at 333 mA cm^{-2} and 850 °C under wet CH_4 and wet CBM, respectively.

Table 1. Meancarbon contents of the anode surface and catalyst surface of the cells after the durability tests under wet CH_4 and wet CBM.

Sample	Mean carbon content (at%)	
Surface	Anode surface	Catalyst surface
The freshly-reduced surface	22.4	6.38
(LSCrFO//Ni-YSZ)-CH_4 after ageing test for 100 h	18.61	7.34
(LSCrFO//Ni-YSZ)-CBM after ageing test for 35 h	42.34	7.88

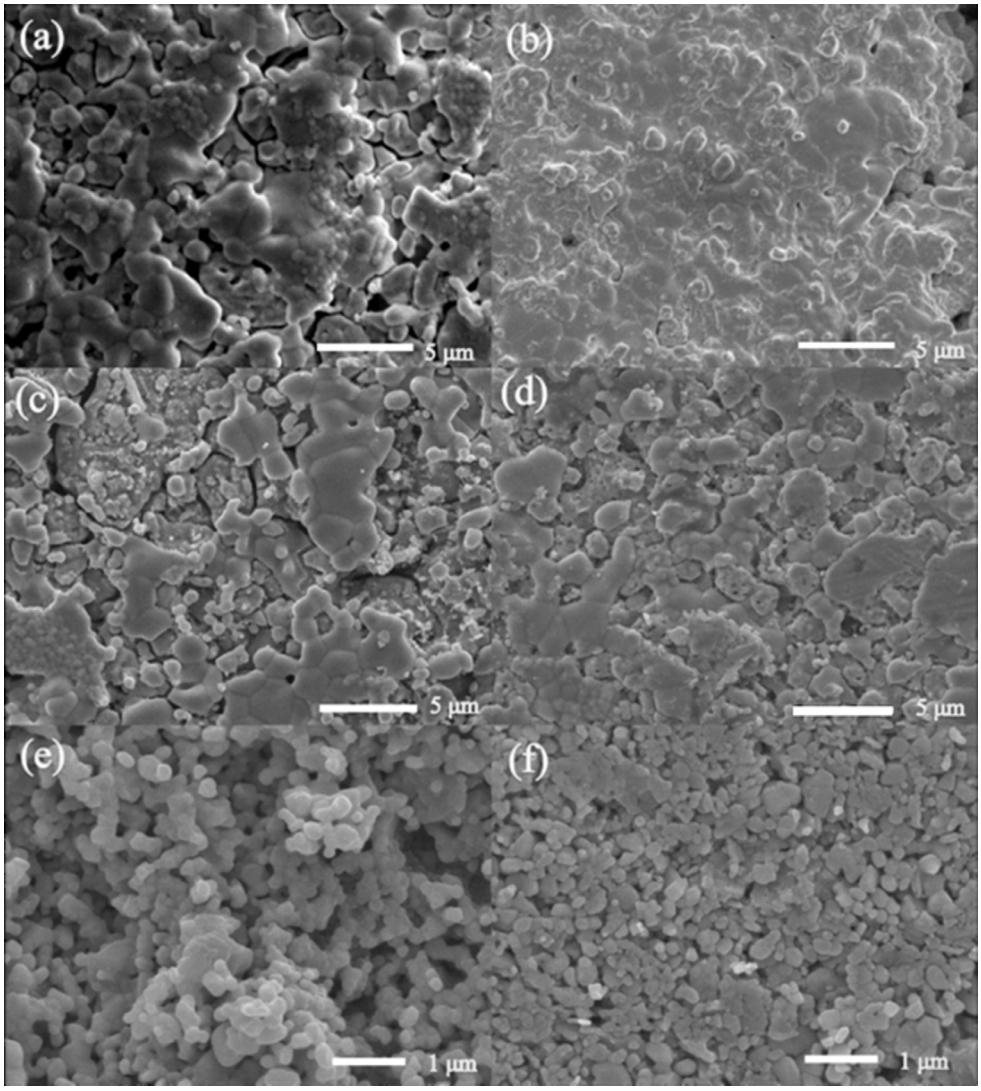

Fig. 10. SEMs of the anode surfaces of the bare cells without the LSCrFO catalyst layer before (a) and after (b) the durability tests under wet CH_4 for 30 min; the anode surface (c,d) and the catalyst surface (e,f) of the modified cell with the LSCrFO catalyst layer after the durability tests under wet CH_4 for 100 h and under wet CBM for 35 h, respectively.

800 °C. In MSR, 1 mol CH_4 and 1 mol H_2O produce 3 mol H_2. Therefore, even if the CH_4 conversion efficiency is low, enough H_2 is produced to supply the cell, considering that the fuel supply is greatly excessive with a flow rate of 80 mL min^{-1} (STP).

4. Conclusions

In summary, a redox-stable perovskite oxide $La_{0.7}Sr_{0.3}Cr_{0.8}Fe_{0.2}O_{3-\delta}$ (LSCrFO) was applied as a protective layer over a Ni-YSZ anode. Compared with the bare cell, the LSCrFO-modified cell shows improved electrochemical performance and good durability when methane-based fuels are used. Porous properties and thickness of the catalyst layer still need to be adjusted to improve coking resistance. The heavy carbon compounds of CBM have adverse effect on SOFC performance and durability.

Supplementary materials

Supplementary material associated with this article can be found, in the online version, at doi:10.1016/j.jechem.2018.12.007.

References

[1] S. Hossain, A.M. Abdalla, S.N.B. Jamain, J.H. Zaini, A.K. Azad, Renew. Sustain. Energy Rev. 79 (2017) 750–764.
[2] L.S. Mahmud, A. Muchtar, M.R. Somalu, Renew. Sustain. Energy Rev. 72 (2017) 105–116.
[3] F. Ramadhani, M.A. Hussain, H. Mokhlis, S. Hajimolana, Renew. Sustain. Energy Rev. 76 (2017) 460–484 76.
[4] Z.U. Din, Z.A. Zainal, Renew. Sustain. Energy Rev. 72 (2017) 1050–1066.
[5] J.E. Zhao, X.Y. Xu, W. Zhou, Z.H. Zhu, J. Mater. Chem. A. 5 (2017) 6494–6503.
[6] T.T. Wan, A.K. Zhu, Y.M. Guo, C.C. Wang, S.G. Huang, H.L. Chen, G.M. Yang, W. Wang, Z.P. Shao, J Power Sources. 348 (2017) 9–15.
[7] W. Wang, C. Su, Y.Z. Wu, R. Ran, Z.P. Shao, Chem. Rev. 113 (2013) 8104–8151.
[8] B. Hua, W.Y. Zhang, M. Li, X. Wang, B. Chi, J. Pu, J. Li, J Power Sources. 247 (2014) 170–177.
[9] H.L. Chen, F. Wang, W. Wang, D.F. Chen, S.D. Li, Z.P. Shao, Appl. Energy. 179 (2016) 765–777.
[10] K.W. Wei, X.X. Wang, R.A. Budiman, J.H. Kang, B. Lin, F.B. Zhou, Y.H. Ling, J. Mater. Sci. 53 (2018) 8747–8765.
[11] W. Wang, H.Y. Zhu, G.M. Yang, H.J. Park, D.W. Jung, C. Kwak, Z.P. Shao, J Power Sources. 258 (2014) 134–141.
[12] B. Hua, M. Li, Y.F. Sun, Y.Q. Zhang, N. Yan, J. Li, T. Etsell, P. Sarkar, J.L. Luo, Appl. Catal. B: Environ. 200 (2017) 174–181.
[13] Y.F. Song, W. Wang, L. Ge, X.M. Xu, Z.B. Zhang, P.S.B. Julião, W. Zhou, Z.P. Shao, Adv. Sci. 4 (2017) 1700337.
[14] M.L. Faro, R.M. Reis, G.G.A. Saglietti, A.G. Sato, E.A. Ticianelli, S.C. Zignani, A.S. Aric, ChemElectroChem. 1 (2014) 1395–1402.
[15] B.B. Niu, F.J. Jin, R.J. Fu, T. Feng, Y. Shen, J.C. Liu, T.M. He, Electrochim. Acta. 274 (2018) 91–102.

[16] B.H. Park, G.M. Choi, Int. J. Hydrog. Energy. 42 (2017) 28559–28566.
[17] Y.F. Sun, J.H. Li, L. Cui, B. Hua, S.H. Cui, J. Li, J.L. Luo, Nanoscale. 7 (2015) 11173–11181.
[18] N. Xu, T.L. Zhu, Z.B. Yang, M.F. Han, Electrochim. Acta. 265 (2018) 259–264.
[19] K. Zhao, Y. Shen, Z. Huang, F. He, G.Q. Wei, A.Q. Zheng, H.B. Li, Z.L. Zhao, J Energy Chem. 26 (2017) 501–509.
[20] L. Zhu, R. Ran, M. Tadé, W. Wang, Z.P. Shao, Asia-Pac. J. Chem. Eng. 11 (2016) 338–369.
[21] H. Chang, H.L. Chen, Z.P. Shao, J. Shi, J.P. Bai, S.D. Li, J. Mater. Chem. A. 4 (2016) 13997–14007.
[22] M. Chen, S. Paulson, V. Thangadurai, V. Birss, J. Power Sources. 236 (2013) 68–79.
[23] L.H. Son, N.X. Phuc, P.V. Phuc, N.M. Hong, L.V. Hong, J Raman Spectrosc. 32 (2001) 817–820.
[24] J.H. Wright, A.V. Virkar, Q. Liu, F.L. Chen, J Power Sources. 237 (2013) 13–18.
[25] Y.F. Sun, J.H. Li, K.T. Chuang, J.L. Luo, J Power Sources. 274 (2015) 483–487.
[26] Y.Q. Zhang, J.H. Li, Y.F. Sun, B. Hua, J.L. Luo, Acs Appl. Mater. Interfaces. 8 (2016) 6457–6463.
[27] N. Danilovic, A. Vincent, J.L. Luo, K.T. Chuang, R. Hui, A.R. Sanger, Chem. Mater. 22 (2010) 957–965.
[28] G.M. Yang, C. Su, Y.B. Chen, M.O. Tade, Z.P. Shao, J. Mater. Chem. A. 2 (2014) 19526–19535.
[29] Y.F. Sun, J.H. Li, M.N. Wang, B. Hua, J. Li, J.L. Luo, J. Mater. Chem. A. 3 (2015) 14625–14630.
[30] T. Montini, M. Bevilacqua, E. Fonda, M.F. Casula, S. Lee, C. Tavagnacco, R.J. Gorte, P. Fornasiero, Chem. Mater. 21 (2009) 1768–1774.
[31] M. Kerstan, M. Muller, C. Russel, Solid State Sci. 38 (2014) 119–123.
[32] P. Liu, J.R. Kong, Q.C. Liu, X.F. Yang, S.G. Chen, J. Solid State Electr. 18 (2014) 1513–1517.
[33] A.M. Amin, E. Croiset, W. Epling, Int. J. Hydrog. Energy. 36 (2011) 2904–2935.
[34] B.B. Niu, F.J. Jin, X. Yang, T. Feng, T.M. He, Int. J. Hydrog. Energy. 43 (2018) 3280–3290.
[35] N. Xu, T.L. Zhu, Z.B. Yang, M.F. Han, J. Mater. Sci. Technol. 33 (2017) 1329–1333.
[36] H.L. Chen, Y.F. Wu, G.M. Yang, J. Shi, W. Zhou, J.P. Bai, S.D. Li and Z.P. Shao, 11, 2018 1459–1466.